



Research Article

# Two-Stage Differential Hydrocarbon Enrichment Mode of Maokou Formation in Southeastern Sichuan Basin, Southwestern China

Xianfeng Liu <sup>1</sup>, Yilin Liang <sup>1</sup>, Jinbao Duan,<sup>2</sup> and Yanping Luo<sup>2</sup>

<sup>1</sup>School of Geosciences, Yangtze University, Wuhan, Hubei 430100, China

<sup>2</sup>Sinopec Exploration Company, Chengdu, Sichuan 610041, China

Correspondence should be addressed to Yilin Liang; [yilinliang0120@outlook.com](mailto:yilinliang0120@outlook.com)

Received 2 May 2022; Accepted 14 June 2022; Published 30 June 2022

Academic Editor: Shuangpo Ren

Copyright © 2022 Xianfeng Liu et al. Exclusive Licensee GeoScienceWorld. Distributed under a Creative Commons Attribution License (CC BY 4.0).

Sichuan Basin is one of the most potential areas for natural gas exploration and development in China. The Maokou Formation in the basin is one of the important gas-bearing layers in southeastern Sichuan. In recent years, several exploration wells have obtained industrial gas flow in the first member of the Middle Permian Maokou Formation (hereinafter referred to as the Permian Mao-1 member of Maokou Formation), revealing that it may become a new field of oil and gas exploration in Sichuan Basin. Drilling and field survey results show that the shale of Maokou Formation in southeastern Sichuan contains eyeball-shaped limestone. Early studies suggest that the Permian Mao-1 member of Maokou Formation in Sichuan Basin is a set of high-quality carbonate source rocks, but ignoring its oil and gas exploration potential as an unconventional shale reservoir similar to the shale. The enrichment regularity of unconventional natural gas has not been studied from the perspective of source-internal accumulation. And there is a lack of analysis of oil and gas enrichment mode. In this study, we took the Permian Mao-1 member of Maokou Formation in southeastern Sichuan as the target layer. Through macroscopic outcrop observation and geochemical analysis and based on unconventional oil and gas enrichment theory, we carried out a study on natural gas enrichment mode of eyeball-shaped limestone of the Permian Mao-1 member of Maokou Formation in Sichuan Basin. The results show that the hydrocarbon enrichment pattern of the Maokou Formation in southeastern Sichuan is different from the accumulation and occurrence process of common unconventional shale gas reservoirs and conventional carbonate reservoirs. It is a special new hydrocarbon accumulation mode between the above two. According to the difference in the charging time of the hydrocarbon, the background of the reservoiring dynamics, and the occurrence state of oil and gas, we divide the two-stage differential enrichment mode of oil and gas, that is, “early intralayer near-source enrichment” and “late interlayer pressure relief adjustment.”

## 1. Introduction

As one of the most potential areas for natural gas exploration and development in China, Sichuan Basin has experienced decades of exploration practice. A total of 300 conventional gas fields have been found (including two giant gas fields, Puguang gas field and AnyueLongwangmiao gas field). The unconventional natural gas resources in the basin are more abundant. Among them, the tight gas resources have achieved industrial production in eastern and western Sichuan. The shale gas was discovered successively in the

Lower Cambrian Qiongzhusi Formation in Wei 5 in 1966 and in the Upper Ordovician Wufeng Formation-Lower Silurian Longmaxi Formation in Yang 63 in the 1980s. In 2010, Wei 201 achieved a strategic breakthrough in the exploration and development of shale gas in the Qiongzhusi Formation and the Wufeng Formation-Longmaxi Formation. In 2014, China's first large-scale shale gas field of 100 billion cubic meters was discovered in the Jiaoshiba area of Fuling, and the production capacity construction target of  $50 \times 10^8 \text{ m}^3/\text{a}$  was implemented, realizing the industrial production of shale gas in Sichuan Basin [1, 2]. With the

completion and putting into production of the “Natural Gas Transmission from Sichuan to East China” project, the rapid development of natural gas exploration and development in Sichuan Basin is manifested in the continuous expansion into new fields. The Maokou Formation is one of the important gas-bearing layers in Sichuan Basin, especially in southeastern Sichuan. Since the breakthrough in the Maokou Formation of Zi 1 (175,800 m<sup>3</sup>/day) in the early 1960s, Longsheng 1 and Fushi 1 in the Fuling-Qijiang area have successively achieved breakthroughs. The Permian Mao-3 member of Maokou Formation at the top obtained industrial gas flow with daily testing production of 206,000 cubic meters and 67,100 cubic meters, respectively. There are 90 natural gas fields in Shapingba area, of which more than 100 gas wells are found in Maokou Formation. The proven geological reserves of Maokou Formation in Sichuan Basin have exceeded  $1000 \times 10^8$  m<sup>3</sup>. In recent years, Jiaoshi 1 in Fuling area has obtained industrial gas flow again in the first member of the Middle Permian Maokou Formation. Its daily production of natural gas is 16,600 cubic meters and stable trial production of natural gas is 4495 cubic meters per day. The Permian Mao-1 member of Maokou Formation is distributed stably in the region, and many wells in it have encountered good oil and gas shows. This shows good exploration prospects for Maokou Formation in the Jiaoshiba area and adjacent areas.

Through drilling and field survey, we found that the shale of the Permian Mao-1 member of Maokou Formation in southeastern Sichuan contained eyeball-shaped limestone. Eyeball-shaped limestone is a subnodule of nodular limestone according to the appearance and genetic differences of the tumor or nodule. It is named after its shape like an eyeball [3, 4]. It is a carbonate rock with special structure, which belongs to the category of limestone-marl alternations [5–13]. Differences of weathering resistance ability lead to the appearance of eyeball-shaped structures. It consists of a darker “eyelid” and a lighter “eyeball.” Usually, the interface is clear and can be easily identified in field profiles and cores [14–16]. In the Permian in southern China, such as Yunnan, Guizhou, Sichuan, Chongqing, Hubei, and Anhui, the eyeball-shaped limestone is widely distributed and the thickness is stable [3, 17, 18]. The research on eyeball-shaped limestone is still in its infancy, mainly focusing on the temporal and spatial distribution characteristics and genetic mechanisms [10, 19–30]. The “eyelid” part of the eyeball-shaped limestone is mainly marl-bearing or argillaceous limestone, which has a high abundance of organic matter and is widely distributed vertically and horizontally. It has strong hydrocarbon generation potential and is often regarded as a good source rock [31, 32], and its hydrocarbon-generation potential has attracted great attention from petroleum scientists [33–36]. The dissolution caves or suture lines and cracks in the eyeball-shaped limestone not only provide reservoir space for oil and gas but also become effective migration pathways [37, 38].

Early studies mainly regarded the Permian Mao-1 member of Maokou Formation in Sichuan Basin as a set of carbonate source rocks from the perspective of conventional oil and gas [33], ignoring its oil and gas exploration potential

as a shale-like unconventional reservoir. The study of unconventional natural gas enrichment law from the perspective of source-internal accumulation has not been carried out, and the analysis of oil and gas enrichment modes is lacking. In this study, the first member of Maokou Formation in southeastern Sichuan was taken as the target strata. Through macroscopic field outcrop observation and geochemical analysis, based on the unconventional oil and gas enrichment theory, the enrichment mode of eyeball-shaped limestone natural gas in the Permian Mao-1 member of Maokou Formation in Sichuan Basin was studied.

## 2. Geological Setting

Sichuan Basin is located in the west of the Yangtze platform (southwest of China), with a total effective exploration area of about  $19 \times 10^4$  km<sup>2</sup>. It is a large superposition basin mainly containing natural gas and supplemented by oil [39, 40] (Figure 1(a)). Since the Sinian, Sichuan Basin has experienced multistage structural movements, forming the current tectonic framework surrounded by mountains on all sides [41]. The basin as a whole presents the rhombic structural characteristics of NE extension. From Sinian to Middle Triassic, marine carbonate rocks were deposited, and from Late Triassic to Eocene, continental clastic rocks were deposited [42, 43] (Figure 1(b)). The study area is located in the Fuling area of southeastern Sichuan. Structurally, it belongs to the Bashansi syncline in the Wanxian syncline of the high-steep fold belt in eastern Sichuan. The structural axis is generally arc-shaped in the northwest direction, and the longitudinal direction is an asymmetrical syncline with a steep southeast flank and a gentle northwest flank [44, 45] (Figure 1(c)).

Before the deposition of the Permian, the Caledonian movement and the Yunnan movement caused the basin to suffer long-term denudation under the action of uplift, thus forming a quasiplainized gentle-slope-type sedimentary basement. A global transgression event occurred at the initial stage of the Early Permian, causing the entire Upper Yangtze landmass to be submerged to form a set of carbonate ramp deposits. At the end of the Early Permian, the basin was uplifted under the influence of the Soochow Movement, and the Middle Permian strata were denuded to varying degrees. As a result, a regional unconformity surface was formed at the top boundary of the Maokou Formation, and the bottom boundary was conformably overlaid on the carbonate rocks of the Qixia Formation. The weathering crust karst fracture-cave reservoir was formed in this stage [46, 47]. The thickness of the Permian Mao-1 member of Maokou Formation ranges from 100 m to 140 m, and the overall distribution pattern is thick in the southwest and thin in the northwest (Figure 1(d)). The lithology of Jiaoye 66-1 and Lengshuixi profile is mainly eyeball-shaped limestone and also includes various composite bedding rhythm layers composed of interbedded limestone and mudstone, such as middle massive limestone, vein-like bedding marl rock, lenticular bedding calcareous mudstone, and laminar bedding calcareous mudstone (Figure 2).

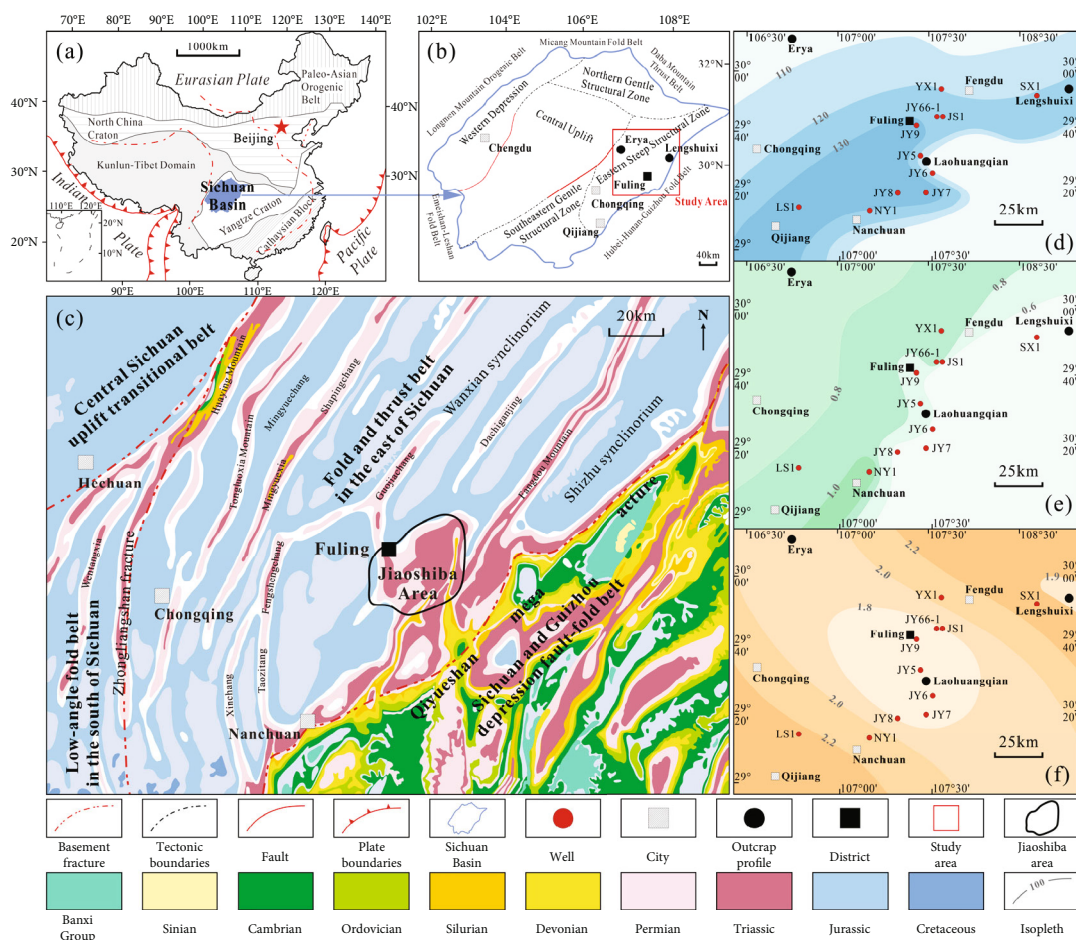


FIGURE 1: (a) Geographic location of the Sichuan Basin in southwestern China. (b, c) Location map showing the tectonic units of Sichuan Basin and the study area in the southeast region [45]. (d) Stratigraphic thickness contour map of Permian Mao-1 member of Maokou Formation in Fuling and adjacent areas. (e) Variation map of TOC average value distribution of Permian Mao-1 member source rocks in main exploration wells and outcrop profiles in the study area. (f) Ro contour map of Permian Mao-1 member of the Maokou Formation source rock in the study area. LS = Longsheng; NY = Nanye; JY = Jiaoye; JS = Jiaoshi; YX = Yongxing; SX = Sanxing.

During the sedimentary period of the Middle Permian, the organisms flourished and the organic matter content was abundant. The average TOC values of the Permian Mao-1 member of Maokou Formation source rocks in the exploration wells and outcrops in the study area are distributed between 0.51% and 0.89%, which are all higher than the lower limit of TOC of effective source rocks. And the distribution in the area is high in the middle and low on both sides (Figure 1(e)). The maturity of source rocks varies greatly. The  $R_o$  value of source rocks in the Jiaoshiba area is relatively low, distributed in the range of 1.66%–1.69%, in the middle-late stage of high maturity. The source rocks in the southwest and northeast have higher  $R_o$  values, higher than 2.0%, and are in the overmaturity stage (Figure 1(f)).

### 3. Experimental Samples and Methods

The organic geochemical analysis data of source rocks and natural gas in this experiment were all from the Key Laboratory of “Oil and Gas Resources and Explora-

tion Technology” of the Ministry of Education of Yangtze University.

In this study, the Lengshuixi profile and Jiaoye 66-1 in southeastern Sichuan were systematically sampled, and the fluid inclusion petrographic observation, composition analysis, and temperature-salinity test were carried out. The preparation and measurement of the samples were performed in an environment with humidity of 30% and temperature of 20°C. Controlled by complex factors, such as the genesis and destruction of inclusions, objects that conform to the FIA concept were screened out for measurement and analysis to ensure the reliability of the information [48–50]. A Nikon Eclipse 80i dual-channel fluorescence-transmitted light microscope equipped with transmitted light (TR) and ultraviolet light (UV) was used to detect fluid inclusions in the sample. The excitation wavelength of the ultraviolet light was 330–380 nm. For the gas inclusions in the sample, a LabRAM HR800 laser Raman spectrometer was used to nondestructively characterize the gas-phase components of a single inclusion larger than 1  $\mu\text{m}$  using a YAG solid-state laser at a wavelength of 532 nm. We selected hydrocarbon inclusions and coeval aqueous

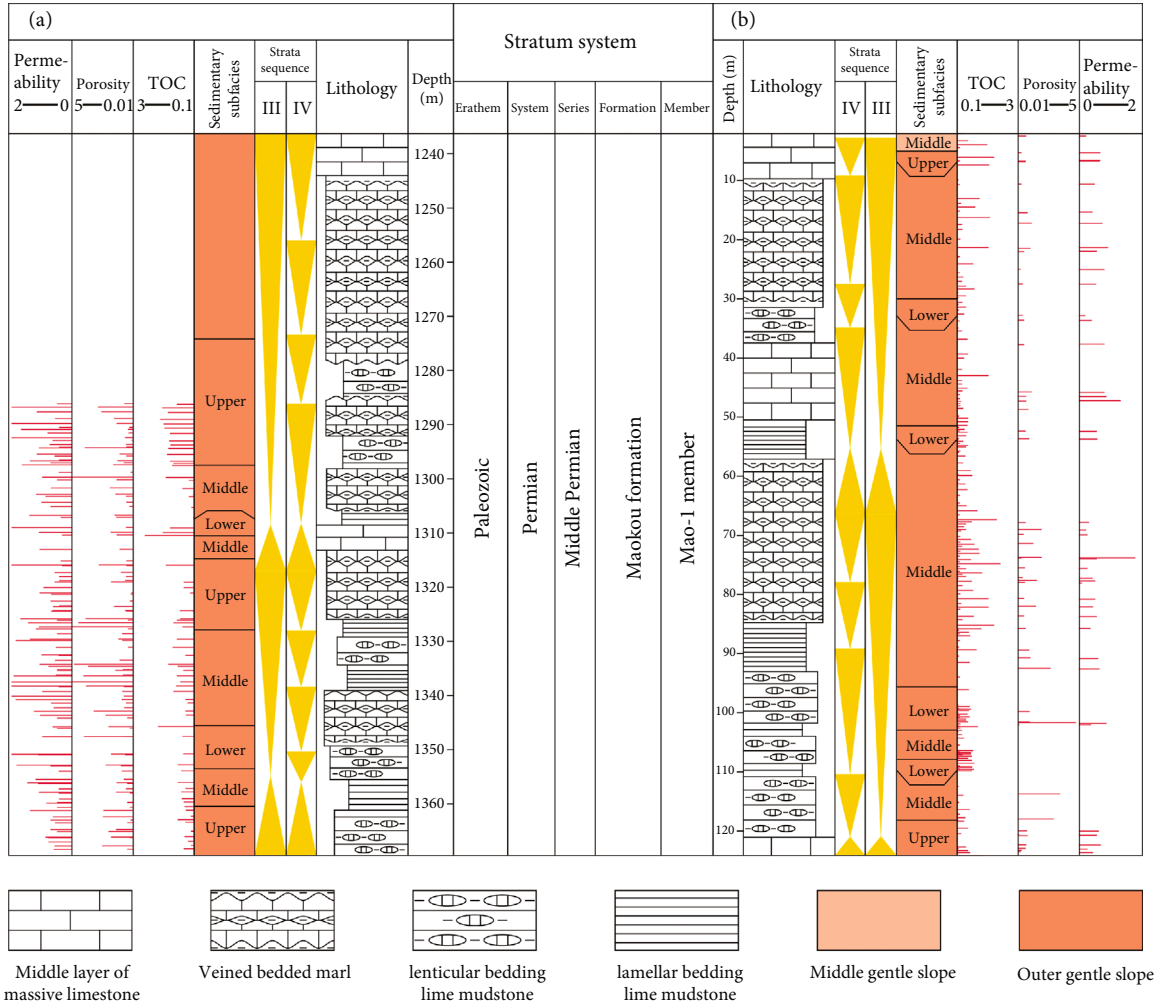


FIGURE 2: The comparison of sedimentary bedding in Permian Mao-1 member of the Maokou Formation between (a) JY 66-1 and (b) Shizhu Lengshuixi profile. JY = Jiaoye.

inclusions from different periods to measure the homogenization temperatures. The measured homogenization temperatures of the coeval aqueous inclusions can approximately represent the stratigraphic temperature when the hydrocarbon inclusions are trapped. The homogenization temperature ( $T_h$ ) and freezing point temperature ( $T_m$ ) of the fluid inclusions were measured using a Linkam THMSG600 micro cooling-heating stage and by applying the thermal cycling method according to Goldstein and Reynolds [49]. The heating rate used to measure the value of  $T_h$  was  $10^\circ\text{C}/\text{min}$  ( $50^\circ\text{F}/\text{min}$ ). The amount of salt (salinity) in the trapped fluid was determined at a heating/cooling rate of  $1^\circ\text{C}/\text{min}$  of salinity ( $33.8^\circ\text{F}/\text{min}$ ). The temperature accuracy for measuring  $T_h$  and  $T_m$  was  $-1^\circ\text{C}$  ( $33.8^\circ\text{F}$ ) and  $-0.1^\circ\text{C}$  ( $32.2^\circ\text{F}$ ), respectively. Using the linear relationship between the Raman spectral shift of the methane system and the pressure in the fluid inclusions found by Lu et al. [51], we quantitatively characterized the pressure evolution process of the Permian Mao-1 member of Maokou Formation in the Lengshuixi profile.

The relationship among fluid inclusion homogenization, laser Raman shift, and inclusion trapping pressure in this

study was obtained by calculating the inclusion density ( $\rho$ ) using the Raman scattering peak ( $\nu_1$ ) of methane inclusions. We used the formula obtained by Lu et al. [51] based on the experimental results fitting the methane Raman scattering peak ( $\nu_1$ ) shift and the methane density ( $\rho$ ) with a good linear relationship, which is suitable for the density calculation of methane inclusions with methane content of 90-100%, and the correlation coefficient is 0.9987:

$$\rho = -5.17331 \times 10^{-5} D^3 + 5.53081 \times 10^{-4} D^2 - 3.51387 \times 10^{-2} D, \tag{1}$$

where  $\rho$  is the density of methane inclusions,  $\text{g}/\text{cm}^3$ ;  $D = \nu_1 - \nu_0$ ,  $\nu_1$  is the measured methane Raman scattering peak of methane inclusions, and  $\nu_0$  is the methane Raman scattering peak of methane inclusions when the pressure is close to 0. Affected by laboratory calibration methods, the value of  $\nu_0$  is different in different laboratories. In this paper, the value of  $\nu_0$  is calibrated by the Raman Laboratory in the Key Laboratory of the School of Geosciences, Yangtze University.

The calculation of the inclusion trapping pressure is based on the equation of state for supercritical methane systems established by Duan et al. (1992a, 1992b) [52]:

$$Z = \frac{PV}{RT} = \frac{PrV_r}{Tr} = 1 + \frac{B}{V_r} + \frac{C}{V_r^2} + \frac{D}{V_r^4} + \frac{E}{V_r^5} + \frac{F}{V_r^2} \left( \beta + \frac{\gamma}{V_r^2} \right) \exp \left( \frac{\gamma}{V_r^2} \right), \quad (2)$$

where  $B = a_1 + (a_2/T_r^2) + (a_3/T_r^3)$ ;  $C = a_4 + (a_5/T_r^2) + (a_6/T_r^3)$ ;  $D = a_7 + (a_8/T_r^2) + (a_9/T_r^3)$ ;  $E = a_{10} + (a_{11}/T_r^2) + (a_{12}/T_r^3)$ ;  $F = \alpha/T_r^3$ ;  $P_r = P/P_c$ ;  $T_r = T/T_c$ ;  $V_r = V/V_c$ ;  $V_c = RT_c/P_c$ ;  $P$  is the pressure (bar);  $T$  is the temperature (K);  $R$  is the gas constant ( $0.08314467 \text{ bar}\cdot\text{dm}^3\cdot\text{K}^{-1}\cdot\text{mol}^{-1}$ );  $V$  is the molar volume, which can be determined by the density of methane inclusions and molar mass,  $\text{dm}^3/\text{mol}$ ;  $Z$  is the compression factor;  $P_r$  and  $T_r$  are the comparative pressure and temperature, respectively, and their dimensions are 1;  $P_c$  and  $T_c$  are critical pressure (46 bar) and critical temperature (190.4 K), respectively, and the unit is the same as  $P$  and  $T$ ;  $a_1 = 0.0872553928$ ;  $a_2 = -0.752599476$ ;  $a_3 = 0.375419887$ ;  $a_4 = 0.0107291342$ ;  $a_5 = 0.0054962636$ ;  $a_6 = -0.0184772802$ ;  $a_7 = 0.000318993183$ ;  $a_8 = 0.000211079375$ ;  $a_9 = 0.0000201682801$ ;  $a_{10} = -0.0000165606189$ ;  $a_{11} = 0.000119614546$ ;  $a_{12} = -0.000108087289$ ;  $\alpha = 0.0448262295$ ;  $\beta = 0.75397$ ;  $\gamma = 0.077167$ .

We used field outcrop and drilling core samples to conduct X-diffraction experiments on whole rock and clay minerals to analyze mineral components and find out the content and composition of brittle minerals and clay minerals. We also obtained Young's modulus, Poisson's ratio, and triaxial compressive strength of the rock through the longitudinal and transverse deformation of the rock under different confining pressures in the triaxial stress experiment. Then, we used the formula method proposed by Rickman et al. through Young's modulus and Poisson's ratio to obtain the rock brittleness index; the formula is as follows [53]:

$$\begin{aligned} \text{YM\_BRIT} &= \left( \frac{(\text{YMS\_C} - 10)}{(80 - 10)} \right) \times 100, \\ \text{PR\_BIRT} &= \left( \frac{(\text{PR\_C} - 0.4)}{(0.15 - 0.4)} \right) \times 100, \\ \text{BRIT} &= \frac{(\text{YM\_BRIT} + \text{PR\_BRIT})}{2}, \end{aligned} \quad (3)$$

where YMS\_C is Young's modulus of the rock (104 MPa), PR\_C is Poisson's ratio of the rock, and BRIT is the brittleness index.

The evolution of the adsorbed gas in this study was mainly based on the Langmuir equation to calculate the adsorption capacity at different temperatures and pressures. The Langmuir equation is the equation for calculating shale adsorption:

$$V = VL \times \frac{P}{PL + P}. \quad (4)$$

In the formula,  $V$  represents the adsorption capacity,  $VL$  represents the maximum adsorption capacity of Langmuir,  $P$  represents the pressure, and  $PL$  represents the Langmuir pressure.

## 4. Results and Discussion

**4.1. Early Intralayer Near-Source Enrichment.** The research work has brought about a discovery of the near-source enrichment mode in the middle and early layers of the study area which is similar to the accumulation process of traditional shale gas reservoirs. All are in situ self-generated and self-storage oil and gas accumulation modes. The generated natural gas is adsorbed in the layer or enters the nanoscale pores in a free state [54]. We found that the pore size distribution of nanoscale pores in Maokou Formation reservoirs is dominated by mesopores (2 nm-50 nm), followed by macropores (>50 nm). This is different from the shale gas reservoirs dominated by micropores (<2 nm) of the Silurian Longmaxi Formation in eastern Sichuan. In this study, the high-pressure mercury intrusion curves also indicated micron-scale pores dominated by carbonate intercrystalline pores, which provide good space for the storage of free gas.

In the process of burial and hydrocarbon generation of organic matter, the adsorption effect on the surface of organic matter particles should be satisfied first. After the adsorbed gas is saturated, the free gas will enter the following three types of pores and undergo different degrees of enrichment (Figure 3). First, for the natural gas entering the adjacent talc contraction joints, the accumulation process can be summarized as "adsorption saturation and free occurrence." As a clay mineral, talc has considerable adsorption capacity. Different from the pore size structure dominated by micropores and mesopores of other clay minerals, the pores (contraction joints) generated by talc have a pore size of 160 nm-960 nm, which provided a high-quality storage space for free gas. Therefore, the accumulation state of natural gas in the talc contraction joint should include two types of adsorbed gas and free gas. Secondly, the pore size of the organic matter pores in Jiaoye 66-1 and Lengshuixi profile is relatively large. Although both high-pressure mercury intrusion and nitrogen adsorption detected micropores with a pore size of about 2 nm, the proportion of micropores was less than 5%. The pore size distribution of the organic pores observed under the scanning electron microscope was 2.38 nm-471.5 nm. Therefore, a large amount of free gas exists in the large-diameter organic pores. Finally, in the micron-scale intercrystalline pores characterized by the high-pressure mercury intrusion curve, natural gas is mainly enriched in the free state due to the weak adsorption capacity of calcite.

The gas logging total hydrocarbon content in the Permian Mao-1 member of Maokou Formation of Jiaoye 9 varies greatly. It can be seen from the comprehensive comparison of the stratigraphic profile that the total hydrocarbon content has a good positive correlation with the TOC value, and the peak-valley changes of the contour lines of the two are consistent (Figure 4(a)). The total hydrocarbon contents in the upper layers (2016 m-2143 m) are low, ranging from

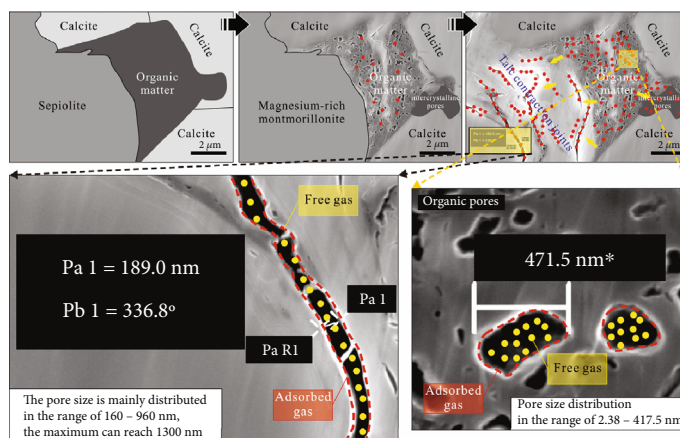


FIGURE 3: The hydrocarbon accumulation mode of the early intralayer near-source enrichment.

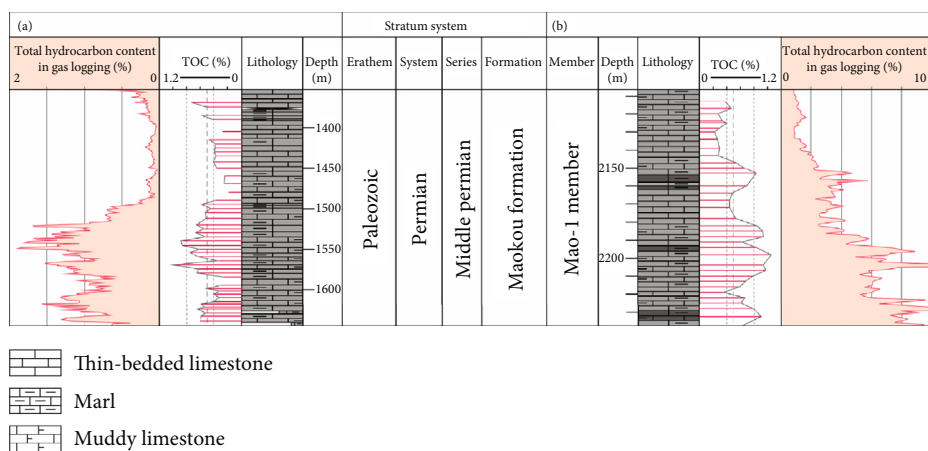


FIGURE 4: There is a good positive correlation between the total hydrocarbon content of the gas-bearing layer and the distribution of TOC values on the profile: (a) Maokou Formation in JY9; (b) Maokou Formation in JY6. JY = Jiaoye.

0.8% to 2.0%. The TOC values in this section are also small, below 0.5%. The total hydrocarbon contents in the middle layers (2143 m-2185 m) increased to 2%-4%, and the TOC values also increased to 0.45%-0.85%. The total hydrocarbon contents in the lower layers (2185 m-2237 m) are the highest, reaching 4%-10%. This section is the most abundant in organic matter, with TOC values in the range of 0.6%-1.0%. The consistency of such changes indicates that there is some genetic relationship between the gas logging total hydrocarbon content and the abundance of organic matter. In the study, we also found that there is a positive correlation between the gas logging total hydrocarbon content and the TOC value in the stratigraphic profile of the Permian Mao-1 member of Maokou Formation in Jiaoye 9, indicating that the gas content of the formation is related to the abundance of organic matter, similar to the characteristic that the production of shale gas is controlled by the content of organic matter. On the one hand, gas source rocks with high organic matter abundance can generate a large amount of oil and gas, and on the other hand, they can develop sufficient organic matter pores and contraction pores to form natural gas storage space. Therefore, the more organic matter richer section, the higher the gas content. We also noticed that the

gas logging total hydrocarbon content of the Maokou Formation in Jiaoye 6 is also positively correlated with the TOC value distribution on the profile (Figure 4(b)). The total hydrocarbon contents in the middle and upper layers (1350 m-1496 m) are very low, all below 0.5%, and the TOC values are also small, mostly below 0.5%. The total hydrocarbon contents in the middle and lower layers (1496 m-1643 m) increased significantly to 0.6%-1.5%, and the TOC values also increased to 0.4%-0.8%. The distribution profiles of total hydrocarbon content and TOC value changing with depth in this well are similar. This shows that the gas-bearing property of the formation depends largely on the abundance of organic matter, which is similar to that of Jiaoye 9. They are typical of intralayer near-source enrichment.

In order to verify the viewpoint of “early intralayer near-source enrichment,” in addition to the above research results, we also collected the following pieces of evidence.

*4.1.1. Interactive Development of Effective Source Rock and Reservoir.* Through field investigation, we found that the Permian Mao-1 member of Maokou Formation in Lengshuixi profile is the most abundant regional layer of chain-

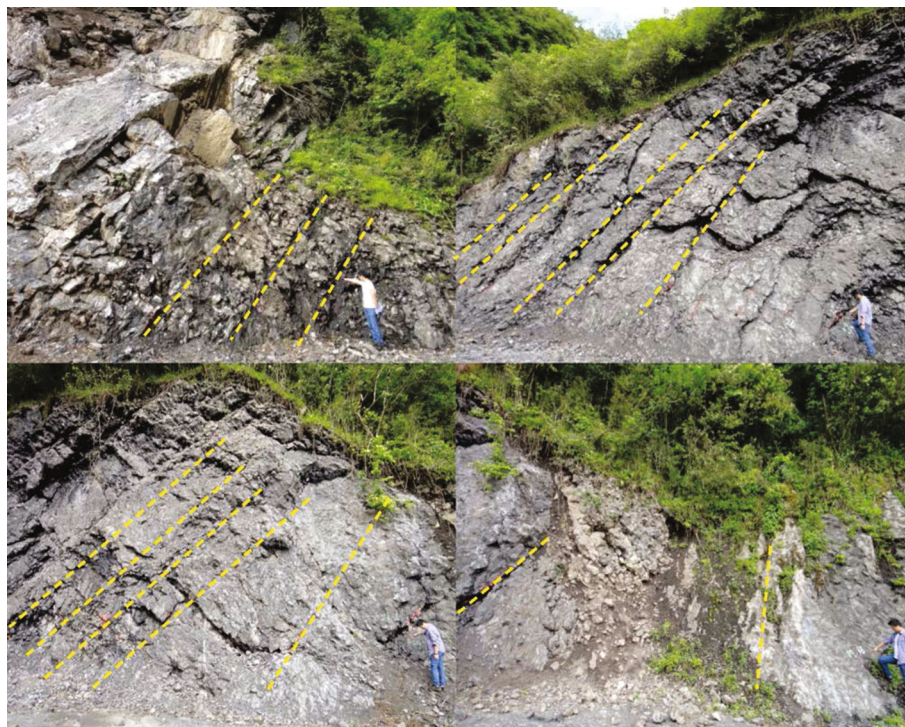


FIGURE 5: Field survey photo of Lengshuixi profile: the Permian Mao-1 member of Maokou Formation rich in eyeball-shaped limestone.

lenticular limestone (eyeball-shaped limestone) (Figure 5). The organic matter of the Permian Mao-1 member of Maokou Formation is mainly contained in the “eyelid structure” of the eyeball-shaped limestone. The test and analysis data of TOC contents showed that the TOC values of the “eyelid structure” part of Jiaoye 66-1 are 0.07%-2.41% (average is 0.83%). The TOC values for the “eyeball structure” part range from 0.03% to 0.88% (average 0.17%). This is very similar to the organic carbon development characteristics of Lengshuixi profile. The TOC values of the “eyelid structure” part in Lengshuixi profile are 0.17%-2.12% (the average is 0.70%). The TOC values for the “eyeball structure” part range from 0.03% to 0.75% (average 0.21%). The average TOC value of the “eyelid structure” in the layers shown in Figure 5 is more than 1.2%, which is the section with the highest organic carbon content in the whole profile.

**4.1.2. Fluid Inclusions Indicate the Nonepisodic Charging of Hydrocarbons.** The microscopic thermometry test results of Jiaoye 66-1 show that the homogenization temperature data points of aqueous inclusions in high-angle calcite veins are distributed in the range of 100°C-160°C. The distribution frequency is relatively even, and there is no obvious accumulation period (Figure 6(a)). This does not conform to the episodic characteristics caused by typical cross-layer migration. To accurately characterize the hydrocarbon accumulation period of the gas reservoir, we performed a combined laser Raman spectroscopy-fluid inclusion test on the Lengshuixi profile (Figure 6(b)). The homogenization temperature of the aqueous inclusions coeval with the methane inclusions in the Lengshuixi profile was obtained (the sampling point is mainly located in the section with the best TOC and phys-

ical properties of the Permian Mao-1 member of Maokou Formation in the Lengshuixi profile) (Figure 6(c)). In accordance with the results of Jiaoye 66-1, the distribution range of homogenization temperature of fluid inclusions in the Lengshuixi profile is 100°C-150°C, and there is no obvious accumulation period. In summary, the charging process of natural gas in the Permian Mao-1 member of Maokou Formation is non-cross-layer migration, which belongs to a steady-state capture process and can be understood as an intralayer near-source enrichment mode.

**4.2. Late Interlayer Pressure Relief Adjustment.** Source rocks in southeastern Sichuan gradually evolved to mature stage during the early deep burial process. By the early Cretaceous, the  $R_0$  value of source rocks (obtained by  $T_{max}$  value conversion) has reached 2.73%-3.27%, generating a large amount of dry gas. Part of this natural gas was adsorbed by organic matter and clay minerals. The other part entered the talc contraction joints of tens to hundreds of nanometers, organic matter pores and micron calcite intercrystalline pores, and was in a free state. In the late Cretaceous, the southeastern Sichuan area was uplifted as a whole, and a large number of reverse faults and folds associated with the faults were formed. As a result, the early formation of oil and gas reservoirs generally suffered from pressure relief adjustments. The pressure of formation fluid controls the preservation of oil and gas reservoirs and the transformation process of adsorbed gas and free gas in the “eyelid structure.” The maximum burial depth of Jiaoye 66-1 can reach 5800 m. During the rapid uplift in the later stage, the adsorption capacity of the reservoir continued to increase. In addition, the pressure relief effect will inevitably lead to the interlayer

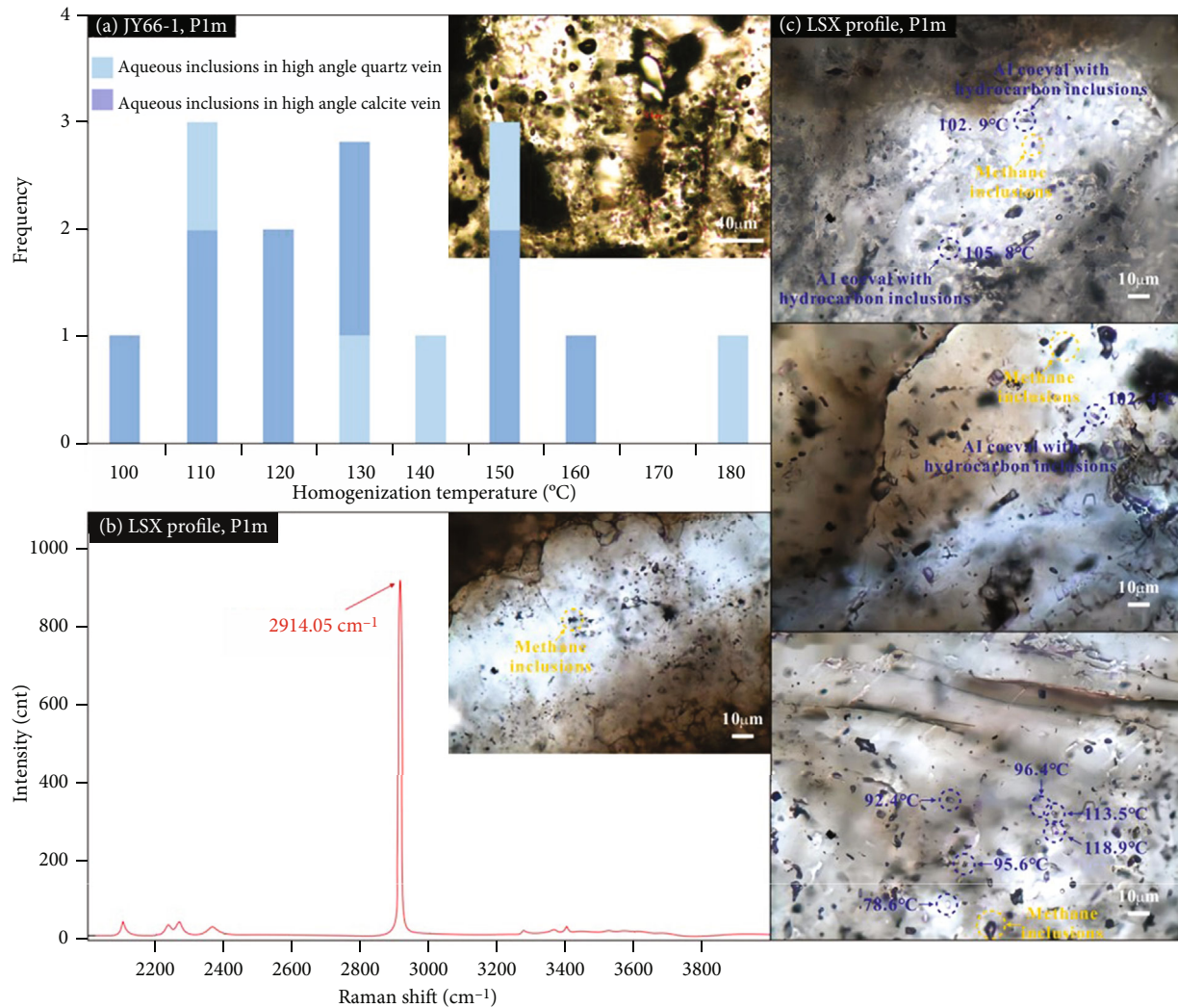


FIGURE 6: Characteristics of fluid inclusions in the study area. (a) The homogenization temperature distribution frequency of aqueous inclusions coeval with the hydrocarbon inclusions in JY66-1. (b) The methane characteristic peak of gas-phase fluid inclusions reflected by microlaser Raman spectroscopy in Lengshuixi profile. (c) The microthermometric characteristics of aqueous inclusions coeval with the hydrocarbon inclusions in Lengshuixi profile. JY = Jiaoye; LSX = Lengshuixi; AI = aqueous inclusions coeval with hydrocarbon inclusions.

adjustment of free gas, forming a conventional gas layer sweet spot in the fracture-rich section.

Before the pressure relief reform, in addition to the natural gas adsorbed on the surface of organic matter and talc, a large amount of free gas was enriched in pores of various grades. The pressure relief process in the late Cretaceous resulted in a shift in the natural gas enrichment state of early gas reservoirs. First, the pressure relief process led to a decrease in the adsorption capacity of organic matter and clay minerals. Part of the adsorbed gas underwent desorption and was transformed into free gas. Second, although the adsorption capacity increased due to the decrease in temperature during the structural uplift, the free gas had already been adjusted. The free gas accumulated in the pores of organic matter and the contraction joints of clay minerals had been greatly reduced, and finally, an unsaturated adsorption state appeared. Then, the fractures and the associated high-angle cracks became important pathways

for free gas (including early free gas and free gas desorbed after pressure relief) to complete the interlayer adjustment. In particular, the high-angle crack system (including reticular cracks) effectively improved the petrophysical properties of the reservoir and promoted the formation of favorable conventional fracture-type “sweet spots” (Figure 7).

The data show that the distribution of gas logging total hydrocarbon content in the Permian Mao-1 member of Maokou Formation in Jiaoshi 1 is special in the stratum section, reflecting that the natural gas obtained in this section is dominated by conventional gas, followed by “shale gas.” The total hydrocarbon contents of the entire formation are generally not high, mostly below 8%. The changing trend is roughly similar to the distribution pattern of TOC values, showing a distribution pattern of higher in the upper part and lower in the lower part. However, there are several abnormally high values (greater than 15%) in the middle and lower layers (Figure 8(a)). Such distribution



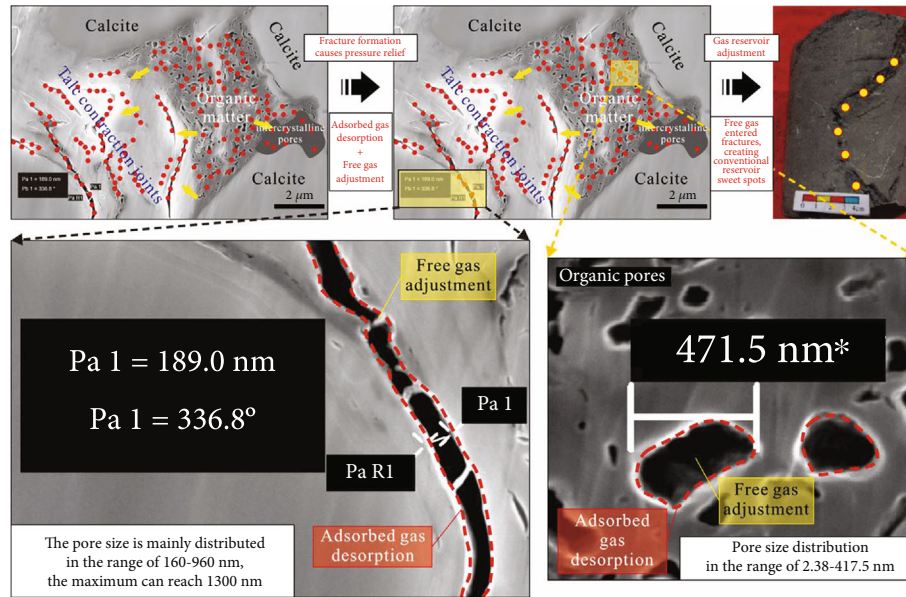


FIGURE 7: The hydrocarbon accumulation mode of the late interlayer pressure relief adjustment.

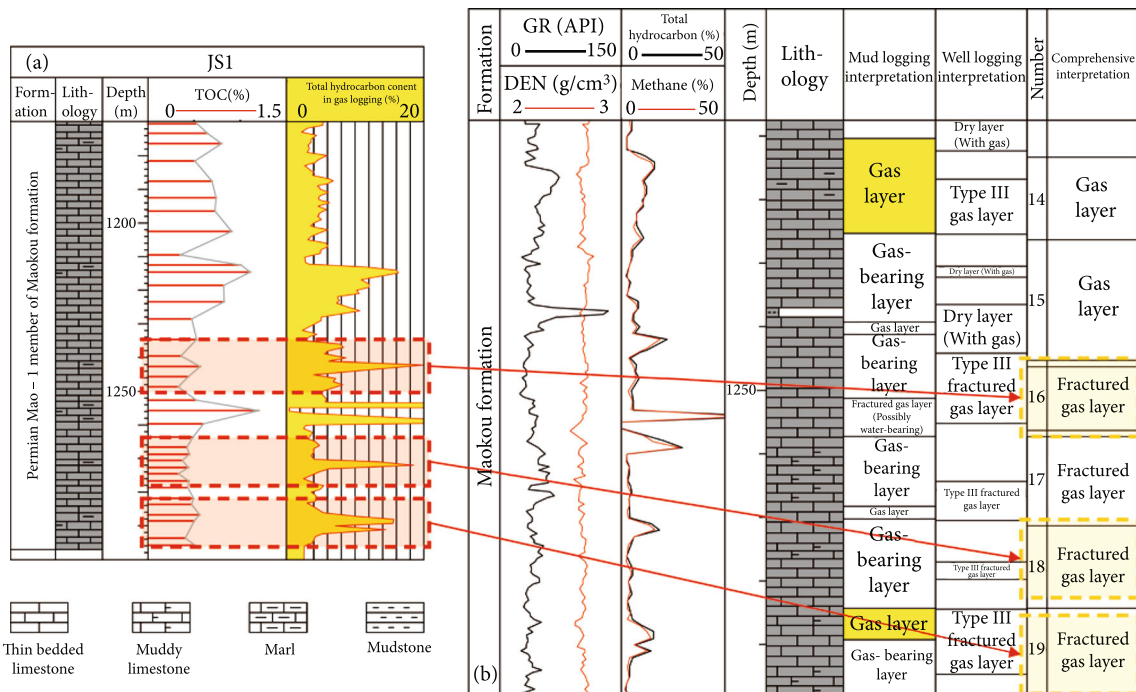


FIGURE 8: (a) Correlation profile between gas logging total hydrocarbon contents and TOC values for Permian Mao-1 member of Maokou Formation in JS1. (b) Comprehensive interpretation diagram of JS1. JS = Jiaoshi.

characteristics suggest that there may be two factors that control the gas content of the formation. One is the abundance of organic matter in source rocks, which is related to hydrocarbon generation and porosity. Similar to the gas content of the “shale gas” layer, it varies with the TOC values. The second is the development zone of pores and cracks in the rocks. The comprehensive logging interpretation of the 1250 m-1297 m industrial gas-producing section in Jiaoshi 1 is all fractured reservoirs (Figure 8(b)). When

drilling into this section, the gas logging total hydrocarbon contents will appear abnormally high (Figure 8). The rock cores were drilled in the whole section of the Permian Mao-1 member of Maokou Formation in Jiaoye 66-1, so the analysis data is relatively systematic. The data show that the gas logging total hydrocarbon contents in the stratum section vary greatly (Figure 9(a)). Several peak protrusions appear on the distribution contour line, which are caused by local gas-bearing pores (holes) and fracture belts. The



FIGURE 9: (a) Correlation profile between gas logging total hydrocarbon contents and TOC values for Permian Mao-1 member of Maokou Formation in JY66-1. Development of fractures at the peak of gas logging in JY66-1: (b) 1297-1302 m and (c) 1363-1365 m. JY = Jiaoye.

Permian Mao-1 member of Maokou Formation in Jiaoye 66-1 has four gas logging peak areas from bottom to top, of which 1363 m-1365 m and 1297 m-1302 m are both gas logging abnormal areas and rich in high-angle cracks and vertical cracks (Figures 9(b) and 9(c)).

In addition to the above research results, the following pieces of evidence on the view of “late interlayer pressure relief adjustment” are made in detail.

**4.2.1. Characteristics of Rock Brittleness.** The X-ray diffraction analysis data (core samples from Jiaoye 66-1 and samples from Lengshuixi outcrop, Erya outcrop, and Lao-huangqian outcrop) show that the carbonate mineral accounts for an average of 72.8%, and the clay mineral content accounts for an average of 18.4% in the Permian Mao-1 member of Maokou Formation (Figure 10(a)). Due to the high mineral contents and good brittleness of

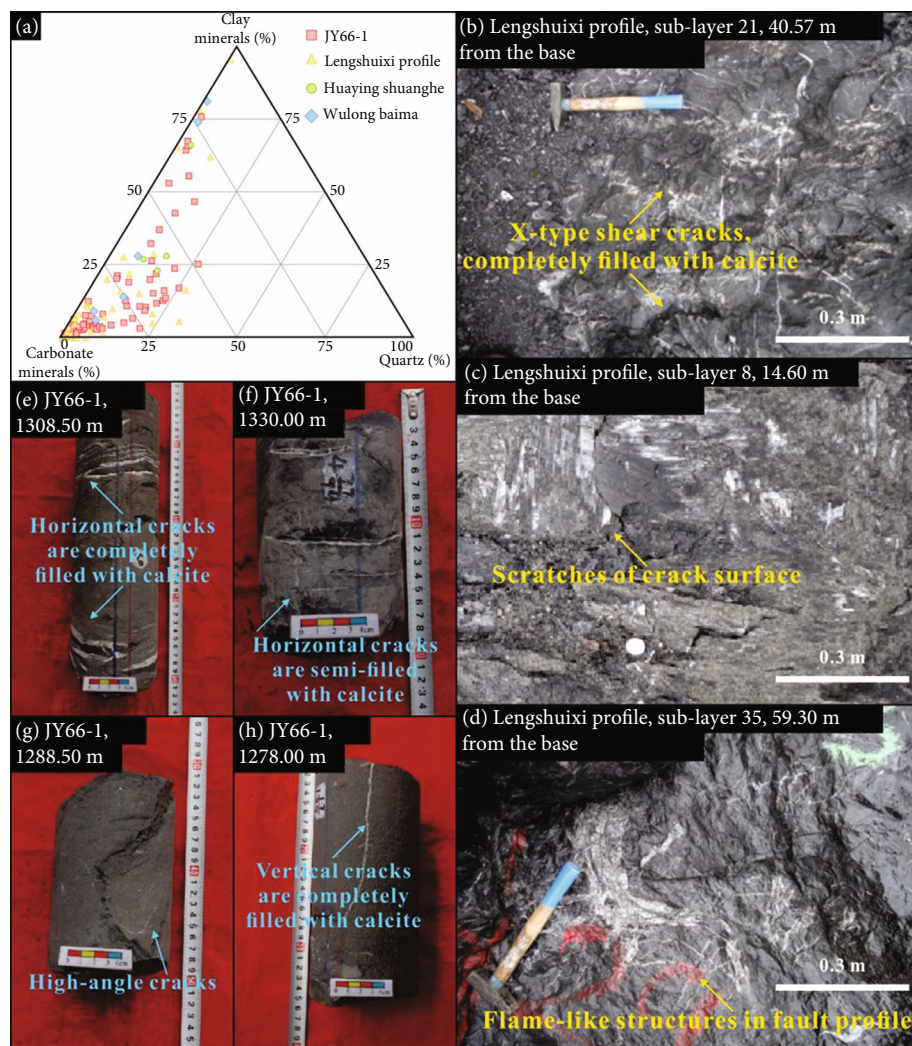


FIGURE 10: (a) Projection point map of mineral X-ray diffraction analysis data of the samples in the study area. (b–h) Macroscopic characteristics of fractures. JY = Jiaoye.

carbonate rocks, artificial fractures are easy to connect with natural fractures and generate induced fractures during fracturing, thus forming complex fracture networks. The calculation results of rock brittleness index also show that the samples (from Lengshuixi profile, Erya profile, and Jiaoye 66-1) of the Permian Mao-1 member of Maokou Formation have strong brittleness under horizontal coring and relatively weak brittleness under vertical coring (Table 1). The average brittleness index of the outcrop samples is 52.20%. The average brittleness index of core samples is 56.26%. The brittleness index of all outcrop samples and core samples is mostly distributed between 50% and 60%, and Young's modulus and Poisson's ratio are low, which proves that the rock brittleness is good.

Through the field outcrop investigation of the macroscopic characteristics of natural fractures, we found that there are X-type shear cracks (Figure 10(b)), scratches of crack surface (Figure 10(c)), and flame-like structures in fault profile (Figure 10(d)) in the Permian Mao-1 member of Maokou Formation of Lengshuixi profile. We observed and described the crack characteristics of rock core samples.

The reservoir fractures of the Permian Mao-1 member of Maokou Formation in Jiaoye 66-1 are vertical cracks (Figures 10(e) and 10(f)), high-angle diagonal cracks (Figure 10(g)), low-angle diagonal cracks, and horizontal cracks (Figure 10(h)). The fracture fillings are mainly calcite, and the crack surface has been filled with bitumen, silicious, pyrite, muddy, and other fillers. The filling method is mainly full filling, followed by different degrees of semifilling. Effective cracks are mainly semifilled cracks, basically no unfilled cracks (Figures 10(e)–10(h)). We counted the opening degree of the cracks from the rock core, mainly distributed at 0.5 mm–1 mm, followed by <0.5 mm as well as between 1 mm–1.5 mm and 1.5 mm–2 mm. The crack opening degree is generally high, which has certain effectiveness in the process of crack formation. We used the drilling core data to count the crack effectiveness. The results showed that full-filling cracks account for about 82%, semifilling cracks account for 18%, and no unfilled cracks were found. It is confirmed that the natural fractures in the target layer of the current study area still have good effectiveness.

TABLE 1: Experiment results of triaxial rock mechanics\*.

## (a) Outcrop samples from Lengshuixi profile and Erya profile

Profile	Lithology	Depth from base (m)	Coring orientation	Confining pressure (MPa)	Compressive strength (MPa)	Young's modulus ( $\times 10^4$ MPa)	Poisson's ratio	Brittleness index
Lengshuixi profile	Gray nodular limestone	14	Horizontal direction 90°	15	273.266	50.268	0.222	64.36
Lengshuixi profile	Gray-black nodular limestone with black calcareous shale	70	Horizontal direction 45°	15	214.440	30.956	0.202	54.57
Lengshuixi profile	Gray limestone with bioclastic nodular argillaceous crystals	20	Horizontal direction 45°	15	233.730	50.232	0.205	67.74
Lengshuixi profile	Gray-black micritic limestone	35	Vertical	15	195.600	50.126	0.225	63.66
Lengshuixi profile	Gray-black nodular limestone	30	Horizontal direction 0°	15	234.825	50.030	0.243	59.99
Lengshuixi profile	Gray-black middle-layered micritic limestone	88	Horizontal direction 0°	15	200.073	30.157	0.224	49.60
Lengshuixi profile	Gray nodular limestone	11	Horizontal direction 90°	15	174.790	50.213	0.300	48.72
Erya profile	Gray nodular limestone	2-1	Vertical	15	102.649	30.219	0.370	20.44
Average value					203.670	40.525	0.248	52.20

## (b) Rock core samples from JY66-1

Well	Lithology	Depth from base (m)	Coring orientation	Confining pressure (MPa)	Peak intensity (MPa)	Elastic modulus (GPa)	Poisson's ratio	Brittleness index
JY66-1	Nodular limestone	—	Horizontal direction 0°	15	163.390	18.800	0.145	57.29
JY66-1	Nodular limestone intercalated with calcareous shale	—	Horizontal direction 45°	15	123.830	14.270	0.161	50.85
JY66-1	Micritic limestone	—	Horizontal direction 90°	15	136.850	15.200	0.149	53.91
JY66-1	Nodular limestone	—	Vertical	15	169.040	18.060	0.162	53.36
JY66-1	Nodular limestone	—	Vertical	15	133.110	16.030	0.130	58.31
JY66-1	Micritic limestone	—	Vertical	15	128.390	15.630	0.140	56.02
JY66-1	Nodular limestone	—	Minimum principal stress direction	15	143.690	18.640	0.123	61.57
JY66-1	Nodular limestone	—	Minimum principal stress direction	15	130.550	18.000	0.134	58.91
JY66-1	Micritic limestone	—	Maximum principal stress direction	15	128.770	14.730	0.113	60.78
JY66-1	Micritic limestone	—	Horizontal direction 0°	15	104.900	15.240	0.143	55.14
JY66-1	Nodular limestone	—	Horizontal direction 45°	15	101.300	14.126	0.154	52.15
Average value					133.070	16.240	0.141	56.26

\*JY = Jiaoye.

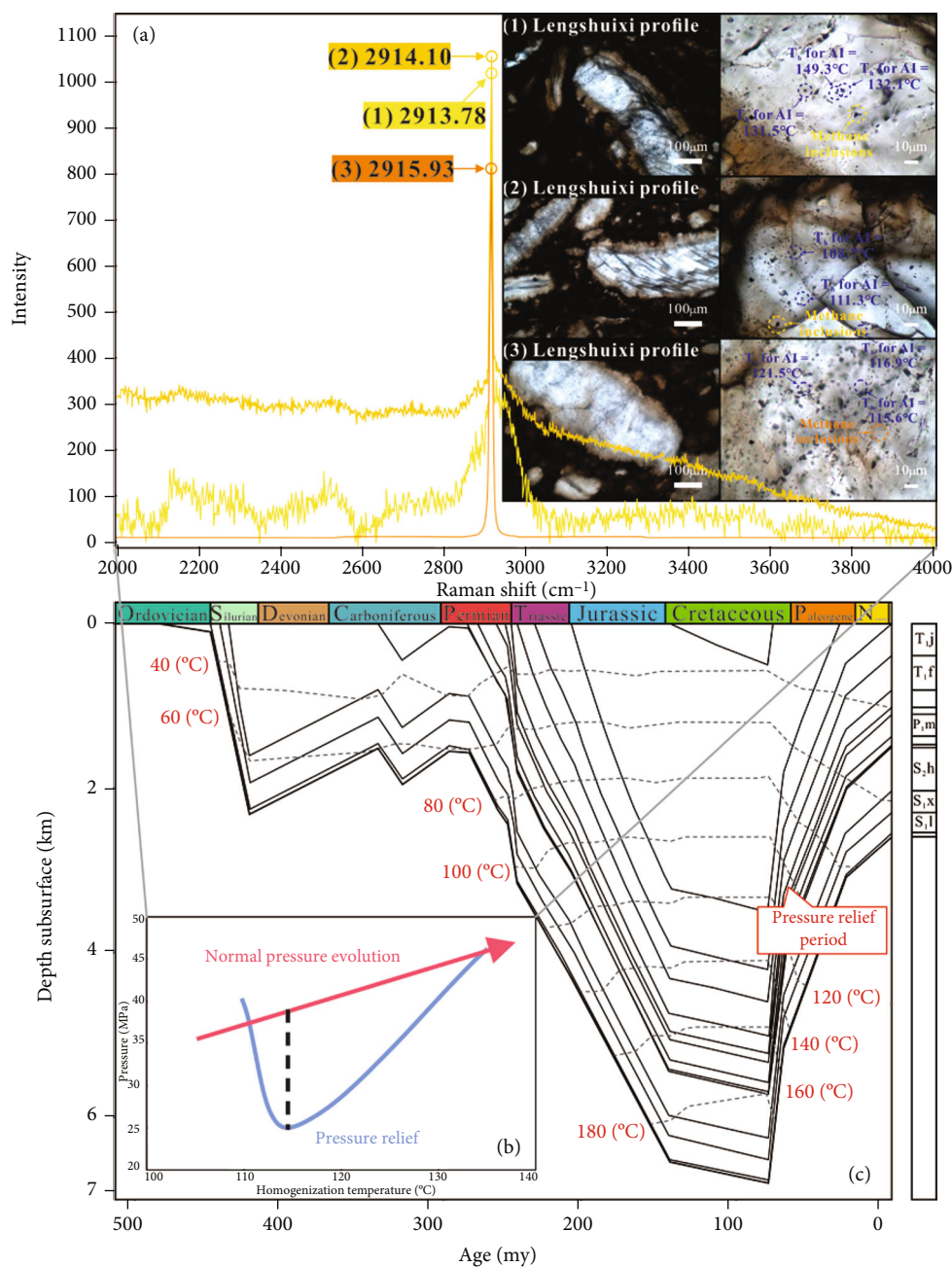


FIGURE 11: (a) The characteristic peak of methane reflected by the laser Raman spectrum of fluid inclusions in Lengshuixi profile. (b) The relationship between pressure evolution and homogenization temperature evolution. (c) The burial-thermal history of JY66-1 reflected that the pressure relief process occurred in the tectonic uplift period after the Cretaceous. Th = homogenization temperature; AI = aqueous inclusions coeval with hydrocarbon inclusions; JY = Jiaoye.

**4.2.2. Laser Raman Spectroscopy Revealed the Pressure Relief Transformation Process.** The test results of fluid inclusions in the Permian Mao-1 member of Maokou Formation of Lengshuixi profile show that the Raman shifts of methane inclusions vary under different homogenization temperatures. When the homogenization temperature of the aqueous inclusions coeval with the methane inclusion is in the range of 130°C–140°C, the Raman shift peak of the methane inclusion is 2913.78 cm<sup>-1</sup>. When the homogenization temperature of the aqueous inclusions coeval with the methane inclusion is in the range of 100°C–110°C, the Raman shift peak of the

methane inclusion is 2914.10 cm<sup>-1</sup>. When the homogenization temperature of the aqueous inclusions coeval with the methane inclusion is in the range of 110°C–120°C, the Raman shift peak of the methane inclusion is 2915.93 cm<sup>-1</sup> (Figure 11(a)). Excluding the influence of experimental instrument calibration and room temperature, the homogenization temperature test results and Raman shift peak characteristics reflect that there is a period of pressure relief experience in the evolution of paleopressure in the gas reservoirs of the Permian Mao-1 member of Maokou Formation in the Lengshuixi profile (Figure 11(b)). Combined with

TABLE 2: Methane adsorption data of JY66-1\*.

Depth (m)	Langmuir volume (m <sup>3</sup> /t)	Langmuir pressure (MPa)	Adsorbed gas volume underground temperature and pressure (m <sup>3</sup> /t)	Water saturation (%)	Adsorbed gas volume with the influence of formation water removed (m <sup>3</sup> /t)
1310.4	1.25	0.94	1.12	20.52	0.89
1322.85	0.91	2.24	0.8	32.53	0.54
1345.44	1.54	2.93	1.31	24.95	0.98
1350.14	1.23	2.39	1.08	19.75	0.87

\*JY = Jiaoye.

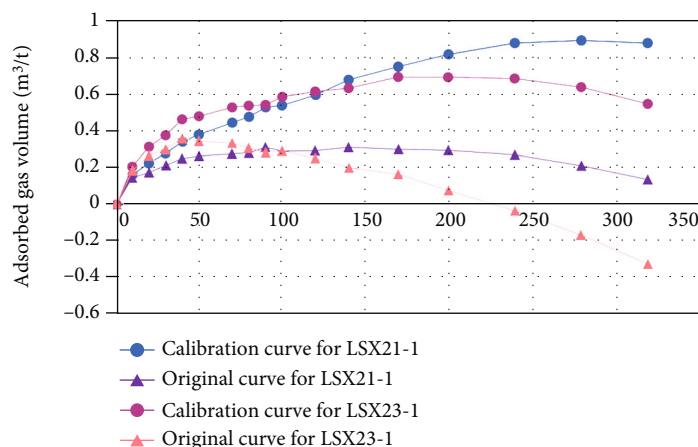


FIGURE 12: Methane adsorption data from Lengshuixi profile. LSX = Lengshuixi.

burial-thermal history, we believe that the pressure relief process occurred in the tectonic uplift stage at the end of Cretaceous (Figure 11(c)). The rapid uplift caused the pressure relief transformation of the early gas reservoir near the fault, forming a large number of associated induced fractures, resulting in the local formation of the fracture type “sweet spot” in Maokou Formation.

**4.2.3. Unsaturated Adsorption State.** The Permian Mao-1 member of Maokou Formation in southeastern Sichuan reached the maximum burial depth in the early Cretaceous, when the source rock had entered the overmature evolution stage. Since the proportion of adsorbed gas with the largest burial depth was the smallest, a large amount of natural gas in the Permian Mao-1 member of Maokou Formation was enriched in pores such as talc contraction joints in free state. During the subsequent tectonic uplift, the formation of faults led to the interlayer adjustment of adsorbed gas and free gas. The pressure decreasing caused the precipitation of adsorbed gas, and a large amount of free gas entered into the conventional reservoir controlled by high-angle cracks for enrichment. Due to the decrease of free gas content in the “eyelid structure,” in the subsequent uplift process, with the increase of reservoir adsorption capacity, the reservoir finally appeared unsaturated adsorption state, that is, the total gas content was less than the maximum adsorption capacity. The gas content test results of the

Permian Mao-1 member of Maokou Formation in Jiaoye 66-1 show that the gas content is 0.21 m<sup>3</sup>/t-0.93 m<sup>3</sup>/t, with an average of 0.51 m<sup>3</sup>/t, and the methane adsorption capacity is about 0.8 m<sup>3</sup>/t (Table 2). Consistent with the test results of the Lengshuixi section (Figure 12), it is confirmed that there is a pressure relief adjustment process of free gas in the Lengshuixi profile and Jiaoye 66-1.

## 5. Conclusions

The characteristics of oil and gas reservoirs, the key period of hydrocarbon generation and accumulation, and the evolution process of paleopressure are comprehensively studied in the Maokou Formation in southeastern Sichuan, and the following conclusions are finally drawn.

The Permian Mao-1 member of Maokou Formation in the Lengshuixi profile is the most abundant regional layer of chain-lenticular limestone (eyeball-shaped limestone). The organic matter of the Permian Mao-1 member of Maokou Formation is mainly contained in the “eyelid structure” of chain-lens limestone (eyeball-shaped limestone). The TOC value of “eyelid structure” was significantly higher than that of “eyeball structure.” We reasonably believe that the “eyelid structure” can be used as an effective source rock, and the “eyeball structure” can be used as a high-quality reservoir, thus forming a mode in which effective source rocks and reservoirs exist interactively.

The hydrocarbon enrichment mode of Maokou Formation in southeastern Sichuan is different from the accumulation and occurrence process of typical unconventional shale gas reservoirs and conventional carbonate reservoirs. It is a special new hydrocarbon accumulation mode between the above two. In this study, a two-stage differential hydrocarbon enrichment mode is divided, namely, “early intralayer near-source enrichment” and “late interlayer pressure relief adjustment.”

During the Early Cretaceous, the natural gas in the study area accumulated near-source within the closed temperature and pressure field. At that stage, the natural gas entered the near-source pore space directly. The hydrocarbon occurrence state was dominated by adsorbed gas in organic matter and clay minerals and free gas in organic pores, talc contraction cracks, and intercrystalline pores. The main controlling factors for such hydrocarbon enrichment mode are TOC and talc content.

During the Late Cretaceous, the formation of faults caused the occurrence of pressure relief. In this stage, the natural gas migrated through the fractures associated with the faults, resulting in interlayer adjustment. The pressure relief effect led to the desorption of the adsorbed gas, which was adjusted to a state of free gas occurrence along the fracture. The fracture-rich layers were dominated by free gas, and there was a small amount of adsorbed gas in organic matter pores and talc contraction cracks.

## Data Availability

All data supporting the results of this study are presented in this paper.

## Conflicts of Interest

The authors declare that they have no conflicts of interest.

## Acknowledgments

This study was funded by the general project of the National Natural Science Foundation of China (No. 42172179).

## References

- [1] D. Z. Dong, S. K. Gao, J. L. Huang, Q. Z. Guang, S. F. Wang, and Y. M. Wang, “Discussion on the exploration & development prospect of shale gas in the Sichuan Basin,” *Natural Gas Industry*, vol. 2, no. 1, pp. 9–23, 2015.
- [2] S. N. He, G. Zong, X. X. Wang et al., “Commercial shale gas development on the fast track: experts discussing the great breakthrough made by Sinopec in the Fuling Shale Play,” *Sinopec Monthly*, no. 4, pp. 27–32, 2014.
- [3] J. X. Luo and Y. B. He, “Origin and characteristics of Permian eyeball-shaped limestones in middle-upper Yangtze region,” *Geological Review*, vol. 56, no. 5, pp. 629–637, 2010.
- [4] H. Z. Wang, Y. L. Chi, Z. J. Zhao, Q. C. Jiang, and W. H. Lu, “Karst reservoirs developed in the Middle Permian Qixia Formation of Sichuan Basin and selection of exploration regions,” *Acta Petrolei Sinica*, vol. 34, no. 5, pp. 833–842, 2013.
- [5] J. X. Yan, “Origin of Permian Chihhsian carbonates from South China and its geological implications,” *Acta Sedimentologica Sinica*, vol. 22, no. 4, pp. 579–587, 2004.
- [6] H. Westphal, “Limestone–marl alternations as environmental archives and the role of early diagenesis: a critical review,” *International Journal of Earth Sciences*, vol. 95, no. 6, pp. 947–961, 2006.
- [7] H. Westphal, F. Hilgen, and A. Munnecke, “An assessment of the suitability of individual rhythmic carbonate successions for astrochronological application,” *Earth-Science Reviews*, vol. 99, no. 1–2, pp. 19–30, 2010.
- [8] J. R. Wheeley, L. Cherns, and V. P. Wright, “Provenance of microcrystalline carbonate cement in limestone–marl alternations (LMA): aragonite mud or molluscs?,” *Journal of the Geological Society*, vol. 165, no. 1, pp. 395–403, 2008.
- [9] S. Boulila, S. Gardin, M. de Rafélis, L. A. Hinnov, B. Galbrun, and P. Collin, “Reply to the comment on “Orbitally forced climate and sea-level changes in the Paleocene Tethyan domain (marl–limestone alternations, Lower Kimmeridgian, SE France)” by S. Boulila, M. de Rafélis, L. A. Hinnov, S. Gardin, B. Galbrun, P.-Y. Collin [Palaeogeography Palaeoclimatology Palaeoecology 292 (2010)57–70],” *Palaeogeography Palaeoclimatology Palaeoecology*, vol. 306, no. 3–4, pp. 252–257, 2011.
- [10] C. Colombié, J. Schnyder, and D. Carcel, “Shallow-water marl–limestone alternations in the Late Jurassic of western France: cycles, storm event deposits or both?,” *Sedimentary Geology*, vol. 271–272, pp. 28–43, 2012.
- [11] X. T. Liu, J. X. Yan, and W. Q. Xue, “Differential diagenesis of limestone–marl alternations,” *Geological Review*, vol. 58, no. 4, pp. 627–635, 2012.
- [12] X. T. Liu, J. X. Yan, Z. X. Ma, and W. Q. Xue, “Origination of limestone–marl alternations from Qixia formation of South China,” *Earth Science*, vol. 39, no. 2, pp. 155–164, 2014.
- [13] C. E. A. Amberg, T. Collart, W. Salenbien et al., “The nature of Ordovician limestone–marl alternations in the Oslo-Asker District (Norway): witnesses of primary glacio-eustasy or diagenetic rhythms?,” *Scientific Reports*, vol. 6, no. 1, pp. 1–13, 2016.
- [14] A. Munnecke and H. Westphal, “Shallow-water aragonite recorded in bundles of limestone–marl alternations—the Upper Jurassic of SW Germany,” *Sedimentary Geology*, vol. 164, no. 3–4, pp. 191–202, 2004.
- [15] A. Munnecke and H. Westphal, “Variations in primary aragonite, calcite, and clay in fine-grained calcareous rhythmites of Cambrian to Jurassic age— an environmental archive?,” *Facies*, vol. 51, no. 1–4, pp. 592–607, 2005.
- [16] A. M. Samet, M. Reolid, A. Marok, and S. Kamikuri, “Environmental conditions during the deposition of the diatomite–organic-rich marl alternation of the lower Messinian of the Lower Chelif Basin (Algeria) interpreted from microfossil assemblages and geochemistry,” *Journal of African Earth Sciences*, vol. 190, article 104521, 2022.
- [17] H. J. Li, X. N. Xie, J. H. Huang, H. Chen, and Z. L. Lin, “Main factors controlling the formation of excellent marine source rocks in Permian Maokou formation of northwest Sichuan, China,” *Earth Science*, vol. 37, no. 1, pp. 171–180, 2012.
- [18] J. X. Luo and Y. B. He, “Characteristics of the Permian source rocks in the middle and upper Yangtze region,” *Natural Gas Geoscience*, vol. 25, no. 9, pp. 1416–1425, 2014.
- [19] F. Böhm, H. Westphal, and S. Bornholdt, “Required but disguised: environmental signals in limestone–marl alternations,”

- Palaeogeography Palaeoclimatology Palaeoecology*, vol. 189, no. 3-4, pp. 161–178, 2003.
- [20] J. Biernacka, K. Borysiuk, and P. Raczynski, “Zechstein (Cal) limestone-marl alternations from the North-Sudetic Basin, Poland: depositional or diagenetic rhythms?,” *Geological Quarterly*, vol. 49, no. 1, pp. 1–14, 2005.
- [21] S. Banerjee and S. Jeevankumar, “Facies and depositional sequence of the Mesoproterozoic Rohtas limestone: eastern Son valley, Vindhyan basin,” *Journal of Asian Earth Sciences*, vol. 30, no. 1, pp. 82–92, 2007.
- [22] J. X. Luo, Y. B. He, D. Wang et al., “Petrological characteristics and sedimentary environment analysis of the Permian of Daxiakou section, Xingshan County, Hubei Province,” *Journal of Palaeogeography (Chinese Edition)*, vol. 4, no. 4, pp. 393–404, 2009.
- [23] X. Zhang, C. M. Lin, H. F. Ling et al., “Nodular limestone and its genesis from the Ordovician Yanwashan Formation in western Zhejiang Province,” *Journal of Palaeogeography (Chinese Edition)*, vol. 11, no. 5, pp. 481–490, 2009.
- [24] B. Badenas, M. Aurell, J. C. Garcia-Ramos, B. Gonzalez, and L. Pinuela, “Sedimentary vs. diagenetic control on rhythmic calcareous successions (Pliensbachian of Asturias, Spain),” *Terra Nova*, vol. 21, no. 3, pp. 162–170, 2009.
- [25] B. Badenas, M. Aurell, M. Armendariz, I. Rosales, J. C. Garcia-Ramos, and L. Pinuela, “Sedimentary and chemostratigraphic record of climatic cycles in lower Pliensbachian marl-limestone platform successions of Asturias (North Spain),” *Sedimentary Geology*, vol. 281, no. 7, pp. 119–138, 2012.
- [26] B. Q. Lu, J. G. Cai, F. Liu, L. Shao, H. G. Wang, and S. Q. Quan, “Upwelling deposits at the marginal slope of a carbonate platform in Qixia stage and its relation with hydrocarbon source rocks,” *Marine Geology & Quaternary Geology*, vol. 30, no. 5, pp. 109–118, 2010.
- [27] D. Husson, N. Thibault, B. Galbrun et al., “Lower Maastrichtian cyclostratigraphy of the Bidart section (Basque Country, SW France): a remarkable record of precessional forcing,” *Palaeogeography Palaeoclimatology Palaeoecology*, vol. 395, pp. 176–197, 2014.
- [28] J. S. Eldrett, C. Ma, S. C. Bergman et al., “Origin of limestone-marlstone cycles: astronomic forcing of organic-rich sedimentary rocks from the Cenomanian to early Coniacian of the cretaceous Western interior seaway, USA,” *Earth and Planetary Science Letters*, vol. 423, pp. 98–113, 2015.
- [29] J. Li, Z. X. Cai, H. R. Chen et al., “Influence of differential diagenesis on primary depositional signals in limestone-marl alternations: an example from middle Permian marine successions, South China,” *Palaeogeography Palaeoclimatology Palaeoecology*, vol. 495, pp. 139–151, 2018.
- [30] C. P. Su, F. Li, X. C. Tan et al., “Recognition of diagenetic contribution to the formation of limestone-marl alternations: a case study from Permian of South China,” *Marine and Petroleum Geology*, vol. 111, pp. 765–785, 2020.
- [31] X. T. Liu, J. X. Yan, W. Q. Xue, Z. X. Ma, and B. Li, “The geobiological formation process of the marine source rocks in the middle Permian Chihhsia formation of South China,” *Science China (Earth Sciences)*, vol. 57, no. 5, pp. 957–964, 2014.
- [32] J. X. Luo, Y. B. He, M. W. He, and X. H. Chen, “Thoughts on characteristics and origin of the middle Permian eyeball-shaped limestone in South China,” *Journal of Palaeogeography (Chinese Edition)*, vol. 21, no. 4, pp. 613–626, 2019.
- [33] S. P. Huang, Q. C. Jiang, Z. C. Wang, W. Su, Q. F. Feng, and Z. Q. Feng, “Differences between the middle Permian Qixia and Maokou source rocks in the Sichuan Basin,” *Natural Gas Industry*, vol. 36, no. 12, pp. 26–34, 2016.
- [34] C. P. Su, X. C. Tan, X. F. Wang et al., “Characteristics of eyeball-shaped limestone reservoir and its genesis of the middle Permian Maokou formation in East Sichuan Basin,” *Marine Origin Petroleum Geology*, vol. 25, no. 1, pp. 55–62, 2020.
- [35] D. F. Hu, L. J. Wang, H. R. Zhang et al., “Discovery of carbonate source rock gas reservoir and its petroleum geological implications: a case study of the gas reservoir in the first member of middle Permian Maokou formation in the Fuling area, Sichuan Basin,” *Natural Gas Industry*, vol. 40, no. 7, pp. 23–33, 2020.
- [36] P. Qian, H. Guang, Z. Xihua et al., “Organic geochemistry, sedimentary environment, and organic matter enrichment of limestone-marlstone rhythms in the middle Permian northern Sichuan Basin, China,” *Marine and Petroleum Geology*, vol. 134, article 105306, 2021.
- [37] F. Afşar, H. Westphal, and S. L. Philipp, “How facies and diagenesis affect fracturing of limestone beds and reservoir permeability in limestone-marl alternations,” *Marine and Petroleum Geology*, vol. 57, pp. 418–432, 2014.
- [38] C. P. Su, R. Li, G. S. Shi, H. F. Jia, and X. B. Song, “Reservoir characteristics of the first member of middle Permian Maokou formation in Sichuan Basin and its periphery and inspirations to petroleum exploration, SW China,” *Petroleum Exploration and Development*, vol. 48, no. 6, pp. 1329–1340, 2021.
- [39] S. C. Zhang and G. Y. Zhu, “Gas accumulation characteristics and exploration potential of marine sediments in Sichuan Basin,” *Acta Petrolei Sinica*, vol. 5, pp. 1–8, 2006.
- [40] S. B. Chen, Y. M. Zhu, H. Y. Wang, H. L. Liu, W. Wei, and J. H. Fang, “Characteristics and significance of mineral compositions of lower Silurian Longmaxi formation shale gas reservoir in the southern margin of Sichuan Basin,” *Acta Petrolei Sinica*, vol. 32, no. 5, pp. 775–782, 2011.
- [41] S. G. Liu, W. X. Ma, J. Luba, W. M. Huang, X. L. Zeng, and C. J. Zhang, “Characteristics of the shale gas reservoir rocks in the lower Silurian Longmaxi formation, east Sichuan basin, China,” *Acta Petrologica Sinica*, vol. 27, no. 8, pp. 2239–2252, 2011.
- [42] G. Y. Zhu, S. C. Zhang, Y. B. Liang et al., “The characteristics of natural gas in Sichuan basin and its sources,” *Earth Science Frontiers*, vol. 2, pp. 234–248, 2006.
- [43] Y. S. Ma, X. Y. Cai, P. R. Zhao, Y. Luo, and X. F. Zhang, “Distribution and further exploration of the large-medium sized gas fields in Sichuan Basin,” *Acta Petrolei Sinica*, vol. 31, no. 3, pp. 347–354, 2010.
- [44] T. L. Guo and H. R. Zhang, “Formation and enrichment mode of Jiaoshiba shale gas field, Sichuan Basin,” *Petroleum Exploration and Development*, vol. 41, no. 1, pp. 31–40, 2014.
- [45] J. Gao, S. He, J. X. Zhao, and J. Z. Yi, “Geothermometry and geobarometry of overpressured lower Paleozoic gas shales in the Jiaoshiba field, Central China: insight from fluid inclusions in fracture cements,” *Marine and Petroleum Geology*, vol. 83, pp. 124–139, 2017.
- [46] H. Mingyi, H. Zhonggui, W. Guoqi, Y. Wei, and L. Mancang, “Sequence lithofacies paleogeography and reservoir potential of the Maokou formation in Sichuan Basin,” *Petroleum Exploration and Development*, vol. 39, no. 1, pp. 51–61, 2012.



- [47] D. J. Li, H. Chen, H. D. Chen et al., "Relationship between reservoir development in the middle Permian Maokou formation and paleostructure evolution in the Sichuan Basin," *Oil & Gas Geology*, vol. 37, no. 5, pp. 756–763, 2016.
- [48] J. L. R. Touret, "Fluids in metamorphic rocks," *Lithos*, vol. 55, no. 1-4, pp. 1–25, 2001.
- [49] R. H. Goldstein and T. J. Reynolds, "Systematics of fluid inclusions in diagenetic minerals," *Society for Sedimentary Geology Short Course*, vol. 31, p. 199, 1994.
- [50] R. H. Goldstein, I. Samson, A. Anderson, and D. Marshall, "Petrographic analysis of fluid inclusions," *Fluid Inclusions-Analysis and Interpretation*, vol. 32, pp. 9–53, 2003.
- [51] W. J. Lu, I. M. Chou, R. C. Burruss, and Y. C. Song, "A unified equation for calculating methane vapor pressures in the CH<sub>4</sub>-H<sub>2</sub>O system with measured Raman shifts," *Geochimica et Cosmochimica Acta*, vol. 71, no. 16, pp. 3969–3978, 2007.
- [52] Z. H. Duan, N. Møller, and J. H. Weare, "An equation of state for the CH<sub>4</sub>-CO<sub>2</sub>-H<sub>2</sub>O system: I. Pure systems from 0 to 1000°C and 0 to 8000 bar," *Geochimica et Cosmochimica Acta*, vol. 56, no. 7, pp. 2605–2617, 1992.
- [53] R. Rickman, M. J. Mullen, J. E. Petre, W. V. Grieser, and D. Kundert, "A practical use of shale petrophysics for stimulation design optimization: all shale plays are not clones of the Barnett shale," in *SPE Annual Technical Conference and Exhibition*, pp. 1–11, Denver, Colorado, USA, 2008.
- [54] X. X. Wang, J. G. Hou, S. H. Li et al., "Insight into the nano-scale pore structure of organic-rich shales in the Bakken Formation, USA," *Journal of Petroleum Science & Engineering*, vol. 176, pp. 312–320, 2019.